

# Flow in unsaturated random porous media, nonlinear numerical analysis and comparison to analytical stochastic models

Thomas Harter<sup>a,\*</sup> & T.C. Jim Yeh<sup>b</sup>

<sup>a</sup>Hydrology Program; University of California, Davis, Parlier, CA 93648, USA

<sup>b</sup>Department of Hydrology and Water Resources; the University of Arizona, Tucson, AZ85719, USA

(Received 20 May 1997; revised 15 December 1997; accepted 26 March 1998)

This work presents a rigorous numerical validation of analytical stochastic models of steady state unsaturated flow in heterogeneous porous media. It also provides a crucial link between stochastic theory based on simplifying assumptions and empirical field and simulation evidence of variably saturated flow in actual or realistic hypothetical heterogeneous porous media. Statistical properties of unsaturated hydraulic conductivity, soil water tension, and soil water flux in heterogeneous soils are investigated through high resolution Monte Carlo simulations of a wide range of steady state flow problems in a quasi-unbounded domain. In agreement with assumptions in analytical stochastic models of unsaturated flow, hydraulic conductivity and soil water tension are found to be lognormally and normally distributed, respectively. In contrast, simulations indicate that in moderate to strong variable conductivity fields, longitudinal flux is highly skewed. Transverse flux distributions are leptokurtic. The moments of the probability distributions obtained from Monte Carlo simulations are compared to modified first-order analytical models. Under moderate to strong heterogeneous soil flux conditions ( $\sigma_y^2 \geq 1$ ), analytical solutions overestimate variability in soil water tension by up to 40% as soil heterogeneity increases, and underestimate variability of both flux components by up to a factor 5. Theoretically predicted model (cross-)covariance agree well with the numerical sample (cross-)covariances. Statistical moments are shown to be consistent with observed physical characteristics of unsaturated flow in heterogeneous soils. © 1998 Elsevier Science Limited. All rights reserved

*Keywords:* soil water, vadose zone, stochastic analysis, heterogeneity, flow modeling.

## 1 INTRODUCTION

Groundwater recharge, irrigation efficiency, runoff, evapotranspiration, and transport of contaminants, vapors, and solutes in the vadose zone are examples of the diverse and important issues associated with a good understanding of unsaturated flow processes and their spatial variability. Spatial variability of soil texture, saturated and unsaturated hydraulic conductivity, moisture content, and water tension in the unsaturated zone have been reported over the past two decades in numerous field studies. These studies found that the permeability of soils may vary by orders of magnitude

over very short distances (decimeters to meters). Variability in soil moisture content and soil tension is significant with coefficients of variation from less than 10% to more than 50%<sup>17,18</sup>.

To investigate the effect of spatial variability on water movement in the unsaturated zone several stochastic analyses of unsaturated flow problems have been conducted in the past. Using analytical methods, Yeh et al.<sup>53–56</sup> and Mantoglou and Gelhar<sup>29–31</sup> have found that the anisotropy of effective unsaturated hydraulic conductivity is moisture dependent and hysteretic, and that the variability of soil–water pressure and moisture content increases as soils dry out. These findings are consistent with observations of lateral interflow to streams and rivers<sup>60</sup>, extensive lateral

\*Corresponding author.

migration of contaminants<sup>7-9,52</sup> and complex hillslope hydrological processes<sup>33</sup>. Similar analytical approaches have been developed to investigate migration of contaminants in the unsaturated zone<sup>44,45</sup>. While these analyses have advanced our understanding of the effect of heterogeneity and furnished means for estimating effective parameters and variability of soil water flow, they are known to be strictly applicable only to soils with low variability due to first-order approximations and implicit normality assumptions in the derivation of these analytical models.

More recently, Monte Carlo simulations of unsaturated flow have been applied to avoid some of the limitations of analytical stochastic models. Hopmans et al.<sup>26</sup> investigated soil water tension distribution in a shallow unsaturated zone with multiple, stochastically separate soil horizons. Yeh<sup>56</sup> examined the effective hydraulic conductivity in layered soils. Soil water flux variability in a one-dimensional flow domain and the dependence of variability on boundary conditions were the focus of work by Ünlü et al.<sup>46</sup>. Other studies describe the physical dynamics of soil water flow in individual, numerically generated, hypothetical soil profile examples<sup>1,38,41,43</sup>. Because of numerical difficulties most of these studies have been limited to soils with a variance of the unsaturated hydraulic conductivity up to one ( $\sigma_y^2 \leq 1, y = \log K$ , where  $K$  is unsaturated hydraulic conductivity,  $\log$  refers to natural logarithm). In contrast, field measurements indicate that  $\sigma_y^2$  is often as high as 3, sometimes even higher<sup>2,6,28,50,37,48</sup>.

The purpose of this work is to provide a general, comprehensive numerical validation of existing analytical stochastic models for steady state unsaturated flow under a realistic range of soil conditions including high spatial variability, varying degrees of statistical anisotropy, and both dry and wet soil conditions. We illustrate the relationship between abstract stochastic models and physical observations of unsaturated flow in heterogeneous soils to underline the significance of stochastic models in our understanding of soil water dynamics. To alleviate the numerical problems associated with computing soil water flow under conditions of large variability and to reduce overall computational requirements, we use a recently developed efficient numerical approach for the simulation of steady state unsaturated flow in heterogeneous soils<sup>21</sup>. Here, the approach is expanded for the implementation of high resolution Monte Carlo simulations with a large number of realizations. The specific objectives of this paper are to determine and prove the statistical sampling accuracy of the Monte Carlo simulations, to derive joint probability distributions associated with soil-water pressure head, unsaturated hydraulic conductivity, and soil water flux in deep unsaturated soils, to compare their means, variances, and (cross-)correlation functions with those obtained from analytical models, and to link observations of soil water dynamics in individual soil profiles with the statistical results derived here. The study provides important information regarding the validity and limitations of simplified

assumptions commonly employed in stochastic analysis of flow in unsaturated porous media.

## 2 METHODOLOGY

Steady state flow in two-dimensional porous media under variably saturated conditions is governed by Richards equation<sup>25</sup>:

$$\frac{\partial}{\partial x_i} \left[ K_i(h) \frac{\partial(x_z + h)}{\partial x_i} \right] = 0 \quad i = x, z, \quad (1)$$

where  $x_x$  and  $x_z$  are the horizontal and vertical coordinates, respectively.  $x_z$  is positive upward,  $h$  is the matric potential or pressure head (negative for unsaturated conditions). Einstein summation is implied. Specific flux in the  $x_i$  direction is given by Darcy's law:

$$q_i = -K_i(h) \frac{\partial(h + x_z)}{\partial x_i}. \quad (2)$$

In this study, the exponential conductivity model first suggested by Gardner<sup>14</sup> is used to describe unsaturated hydraulic conductivity,  $K$ , as a function of matric potential,  $h$ ,

$$K(h) = K_s \exp(\alpha h), \quad (3)$$

where  $\alpha$  is a pore-size distribution parameter,  $K_s$  is saturated hydraulic conductivity, assumed to be locally isotropic. In agreement with field studies,  $K_s$  and  $\alpha$  are assumed to be random space functions (RSFs) with log-normal distributions<sup>49</sup>. The RSFs  $\log K_s$ ,  $\log \alpha$ ,  $\log K$ ,  $h$ , and  $q$  are expanded to

$$\log K_s(x) = f = F(x) + f'(x) \quad (4)$$

$$\log \alpha(x) = a = A(x) + a'(x)$$

$$\log K(x) = y = Y(x) + y'(x)$$

$$h(x) = H(x) + h'(x)$$

$$q_i(x) = Q_i(x) + q'_i(x),$$

where  $F(x)$ ,  $A(x)$ ,  $Y(x)$ ,  $H(x)$  and  $Q_i(x)$  are the expected values of  $\log K_s(x)$ ,  $\log \alpha(x)$ ,  $\log K(x)$ ,  $h(x)$  and  $q_i(x)$ , respectively, and  $f'(x)$ ,  $a'(x)$ ,  $y'(x)$ ,  $h'(x)$ , and  $q'_i(x)$  are zero-mean, second-order stationary perturbations at location  $x$ . We define the geometric mean of  $\alpha$  by  $\Gamma$ , where  $\Gamma \equiv \exp(A)$ .

The numerical flow model, MMOC2, used in this study and its integration into Monte Carlo simulation is fully described by Harter<sup>22</sup> and Yeh et al.<sup>57</sup>. The numerical model is based on the Galerkin finite element technique using rectangular elements and bilinear shape-functions. The nonlinearity in the flow problem is solved iteratively using a Newton-Raphson scheme and an incomplete LU preconditioned conjugate gradient method. After matric potentials are found from eqn (1) with state eqn (3), MMOC2 solves Darcy's eqn (2) with a Galerkin finite

**Table 1. Input parameters for the various hypothetical soil sites:**  $\sigma_f^2$ : variance of  $f = \ln K_s$ ,  $\sigma_a^2$ : variance of  $a = \log \alpha$ ,  $\rho$ : correlation coefficient between  $f$  and  $a$ ,  $\Gamma$ : geometric mean of  $\alpha$  [ $\text{m}^{-1}$ ],  $\Delta x$ : horizontal discretization of finite elements [m],  $\Delta z$ : vertical discretization of finite elements [m],  $\lambda_{fx}$ : horizontal correlation length of  $f$  [m],  $\lambda_{fz}$ : vertical correlation length of  $f$  [m]. Soils A3, E1 and F2 are identical (isotropic reference soil). Similarly, soils B1, D1 and E3 are identical (anisotropic reference soil). Where no value is indicated, values are identical to the corresponding value for the isotropic reference soil (top row)

Name	$\sigma_f^2$	$\sigma_a^2$	$\rho$	$\Gamma$	$H$	$\Delta x$	$\Delta z$	$\lambda_{fx}$	$\lambda_{fz}$
Reference soil	0.95	0.01	0	1.0	-1.5	0.1	0.1	0.5	0.5
Group A: Isotropic, wet soils with different textural variability									
A1	0.01	$10^{-4}$							
A2	0.11	0.01							
A3	0.95	0.01							
A4	3.6	0.04							
Group B: Anisotropic, wet soils with different textural variability									
B1	0.95	0.01				0.3		3.0	
B2	2.15	0.04				0.3		3.0	
B3	3.6	0.04				0.3		3.0	
Group C: Correlated, anisotropic soils with different mean soil water tension									
C1			1		-1.5	0.3		3.0	
C2			1		-20.0	0.3		3.0	
C3			1		-30.0	0.3		3.0	
Group D: Uncorrelated, anisotropic soils with different mean soil water tension									
D1					-1.5	0.3		3.0	
D2					-10.0	0.3		3.0	
Group E: Wet soils with different anisotropy ratios									
E1						0.1		0.5	
E2						0.15		1.5	
E3						0.3		3.0	
Group F: Isotropic wet soils with different scaled vertical correlation scale $\Gamma\lambda_{fz}$									
F1							0.025		0.125
F2							0.1		0.5
F3				10.0	-1.0				

element method to guarantee a continuous flux field,  $q(x)$ , throughout the domain. A semi-analytical, first-order spectral solution  $h_L$  is used as initial guess of the steady state solution to reduce the computational cost of solving Richards eqn (1) numerically. A complete description and validation of this method is given by Harter and Yeh<sup>21</sup>.

To simulate gravity drainage in deep soils with a water table beyond the reach of the simulation domain, and to account for the unknown boundary conditions at the vertical boundaries of the simulation domain, random Dirichlet type boundaries were imposed. Pressure head on all boundaries is set equal to the linearized first-order perturbation solution,  $h_L$ , obtained individually for each realization of  $f$  and  $a$  *a priori* to the numerical solution. The linear solution,  $h_L$ , is derived from spectral analysis and inverse Fourier transform. It assumes that the flow domain is infinite and stationary. Therefore, the numerical simulations represent a subdomain of a much larger, heterogeneous soil domain under gravity drainage whose boundaries are at least several correlation scales away from the simulated domain. Under those conditions, mean vertical flux is controlled through soil texture and average soil water potential, or more specifically, by  $\Gamma$ ,  $H$ , and the covariance function of  $f$  and  $a$ . Random pressure head boundary conditions are consistent with many field applications because boundary conditions are rarely known with certainty.

Several Monte Carlo simulations (MCS) of two-dimensional, vertical soil cross-sections are implemented to investigate the effect of soil heterogeneity, soil water tension, anisotropy, and pore-size distribution on the variability of head and flux. The hydrological characteristics of the simulated soils are chosen to encompass actual field conditions such as those observed by Wierenga et al.<sup>50,51</sup> near Las Cruces, New Mexico. Exponential covariance functions for  $f$  and  $a$  are assumed. The RSF  $a$  is either perfectly correlated with  $f$  ( $\rho = 1$ ) or independent of  $f$  ( $\rho = 0$ ). These two idealized cases correspond to smallest and largest variability in  $y$ , respectively, for any given variability in  $f$  and  $a$ . At field sites, correlation between  $f$  and  $a$  is typically weak, but not negligible<sup>50,51</sup>. The correlation scale of  $a$  is arbitrarily chosen to be identical to that of  $f$ ,  $\lambda_{fi}$ , where  $i = x, z$ . All MCS are performed on a 64 by 64 finite element mesh representing a soil domain that is 6.4 m deep and between 6.4 and 19.2 m wide. A spectral random field generator<sup>19</sup> (SRFG) is used to assign the values of  $f$  and  $a$  to each element.

Different soil groups are used in this study. Table 1 gives a complete list of input parameters for each simulated soil. The effect of increasing variability in saturated hydraulic conductivity is investigated for isotropic soils (group A) and anisotropic soils with anisotropy ratio  $v = \lambda_{fx}/\lambda_{fz} = 6$  (group B). In these examples,  $a$  and  $f$  are assumed uncorrelated, and the mean soil water tension is -1.5 m (relatively

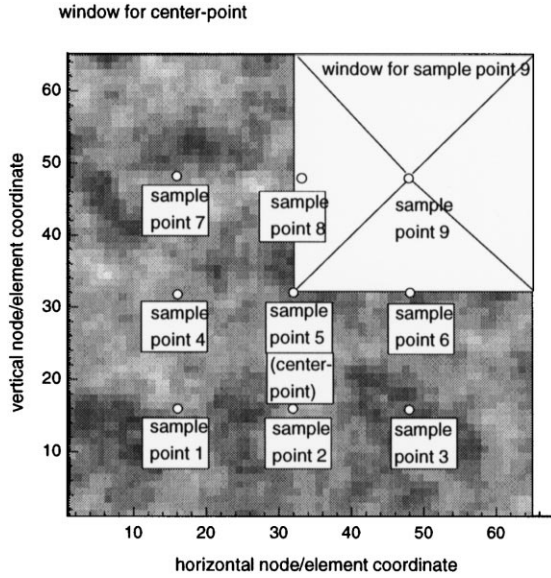


**Fig. 1.** Location of nine sample points (white dots), for which sample covariances and cross-covariances are computed at all lag-distances within a ‘window’ surrounding the sample point. The window is centered on the sample point as shown here for sample point 9. Only the window of sample point 5 is the entire simulation grid, which consists of 64 by 64 elements and 65 by 65 nodes.

wet, representative for a soil at field capacity). Effects of increased dryness is demonstrated for anisotropic soils with  $\nu = 6$ , and either correlated (group C) or uncorrelated  $f$  and  $a$  parameters (group D). Dependence on anisotropy ratio is shown with a series of soils that distinguish each other only through the horizontal correlation scale of  $f$  and  $a$  (group E). Finally, the effect of increasing vertical correlations scale and increasing average pore-size as characterized by  $\Gamma$  is demonstrated through group F of the experiments.

Following Yeh et al.<sup>54</sup>, a first-order analytical solution has been developed<sup>22</sup>. Spectrally derived, analytical solutions for the statistical moments of  $y$ ,  $h$ ,  $q_x$  and  $q_z$  as functions of moments of  $f$  and  $a$  are compared with the Monte Carlo simulation results. A summary of the spectral models is given in Appendix A.

### 3 SAMPLING ACCURACY AND STATIONARITY IN MONTE CARLO SIMULATIONS

#### 3.1 Statistical sampling error of moments

In the MCS, sample mean and variance of the RSFs  $f$ ,  $a$ ,  $y$ ,  $h$ ,  $q_x$  and  $q_z$  are computed by using standard summation<sup>20</sup>. The sample covariance fields and cross-covariance fields  $\text{cov}_{pq}(x_i, \xi)$  around  $x_i$ ,  $i = 1, 1, \dots, 9$ , are evaluated in a window of half the side-length of the simulation domain (Fig. 1). From these nine sample (cross-)covariance fields an average (cross-)covariance

field  $C_{pq}(\xi)$  is obtained

$$C_{pq}(\xi) = 1/9 \sum_{i=1}^9 \text{cov}_{pq}(x_i, \xi). \quad (5)$$

The window for the covariance and cross-variance fields around the center point  $x_c$  of the simulation domain is chosen to be the entire simulation domain to provide additional information on  $\text{cov}_{pq}(x_c, \xi)$  at lag distances up to one-half of the domain size in each direction.

The main weakness of MCS besides numerical inaccuracies is the inherent stochasticity of sample moments. The fundamental theorem of large numbers only guarantees that expected values of the sample moments of an RSF  $g$ ,  $\langle m_g \rangle$ ,  $\langle \text{var}_g \rangle$ , and  $\langle \text{cov}_{gg} \rangle$ , converge in a mean square sense to the ensemble mean  $\mu_g$ , variance  $\sigma_g^2$ , and covariance  $C_{gg}$  of  $g$ . Commonly, the number of realizations necessary to obtain acceptable results is determined by comparing the sample moments of the input parameters (e.g. saturated hydraulic conductivity) with their theoretical, known moments. Sample moments of output RSFs (e.g. head) are assumed to be representative of ensemble moments, when additional realizations do not result in significant changes of output sample moments<sup>4,26,46</sup>. Such qualitative criteria are unsatisfactory, because the number of realizations cannot be determined a priori, and sample moment variability remains unknown. Furthermore, such an approach is not robust against outliers. The use of MCSs for verification of analytical stochastic solutions of porous media flow and transport processes has, therefore, been critically questioned<sup>36</sup>. However, standard statistical theory can be applied to determine the distribution of sample moments a priori. To prove that sample moments determined from Monte Carlo simulation vary according to statistical theory, local sample moment variability within the simulation domain must be compared to those from theory.

For large samples ( $N > 30$ , where  $N$  is the number of realizations) sample moments of a sample from a Gaussian distribution with unknown variance are also Gaussian distributed. The sampling error (i.e. variance)  $\epsilon_m^2$  of the normally distributed sample mean  $m_g$  is<sup>20,27</sup>

$$\epsilon_m^2 = \frac{\sigma_g^2}{N}. \quad (6)$$

$\sigma_g^2$  is not known and must be estimated from the sample variance. The sample variance  $\text{var}_g$  itself has an associated sampling error. For the square root  $s_g$  of  $\text{var}_g$ , the sampling error (i.e. variance)  $\epsilon_s^2$  is approximated by<sup>59</sup>

$$\epsilon_s^2 \approx \frac{\sigma_g^2}{2N}. \quad (7)$$

For the sample variance,  $\text{var}_g$ , simple heuristic considerations lead to the expected sampling error (i.e. standard deviation)  $\epsilon_v$  given  $\epsilon_s^2$

$$\epsilon_v = \frac{(\sigma_g + \epsilon_s)^2 - (\sigma_g - \epsilon_s)^2}{2}. \quad (8)$$

**Table 2. Dimensionless sampling errors for the sample mean (eqn 10) and sample variance (eqn 11) of selected soils**

Soil number with $\sigma_y^2$ , anisotropy ratio, wetness	Mean $y$	Var. $y$	Mean $h$	Var. $h$	Mean $q_x$	Var. $q_x$	Mean $q_z$	Var. $q_z$
A1 0.01/1/wet	1.23	0.99	0.65	0.95	1.10	0.94	1.15	0.98
A2 0.12/1/wet	1.21	0.97	0.62	0.99	1.00	1.07	1.10	1.07
A3 0/86/1/wet	1.21	0.99	0.66	1.09	0.84	1.68	0.97	1.71
A4 3.43/1/wet	1.00	0.97	0.87	1.11	0.83	4.08	0.81	3.87
B1 0.74/6/wet	0.84	0.98	0.23	0.83	0.74	2.38	0.75	1.18
B2 1.76/6/wet	0.84	1.10	0.26	0.98	0.90	5.60	0.74	1.96
B3 3.17/6/wet	0.88	1.19	0.38	1.41	0.98	13.2	0.83	4.25
C1 0.53/6/wet	0.82	0.99	0.23	0.82	0.73	1.97	0.63	1.07
C3 3.12/6/dry	0.67	1.26	0.46	1.20	0.98	–	1.03	–

After substituting for  $\epsilon_s$  from eqn (7), eqn (8) simplifies to:

$$\epsilon_v \approx \frac{2\sigma_g^2}{\sqrt{2N}} \quad (9)$$

eqns (6) and (9) are useful to determine the number of realizations necessary to reduce the sampling error at any given location  $x$  to below a given threshold. For example, the number of realizations necessary to reduce the 95% confidence interval of the sample variance and covariance ( $\pm 2\epsilon_v$ ) to within  $\pm 10\%$  of the ensemble variance and covariance is  $N \geq 800$ . In this study, we use  $N = 1000$ . In addition, advantage is taken of the statistical homogeneity in the random soil properties. Sample mean and sample variance at each location are averaged across the stationary simulation domain.

Proper convergence of the Monte Carlo results is determined a posteriori by computing the variability of the local sample moments across the simulation domain,  $\text{var}(m_g)$  and  $\text{std}(\text{var}_g)$  and by calculating the ratios  $\epsilon'_m = \text{var}(m_g)/\epsilon_m^2$  and  $\epsilon'_v = \text{std}(\text{var}_g)/\epsilon_v$ . These ratios are approximately 1 if sample moment variability is in accordance with eqns (6) and (9). The theoretical sample moments  $\mu_g$  and  $\sigma_g^2$  to compute eqns (6) and (9) are unknown and are estimated from the spatially averaged local sample mean  $\langle m_g \rangle$  and sample variance  $\langle \text{var}_g \rangle$ . Then, the dimensionless sample error of the mean is

$$\epsilon'_m = N \frac{\text{var}(m_g)}{\langle \text{var}_g \rangle} \quad (10)$$

and the dimensionless sample error of the variance is

$$\epsilon'_v = \frac{\sqrt{2N \text{var}(\text{var}_g)}}{2 \langle \text{var}_g \rangle} \quad (11)$$

The following two sections analyze the dimensionless sample errors of both (local and average local) moments in the Monte Carlo simulations performed.

### 3.2 Accuracy of local moments in Monte Carlo simulations

Unsaturated hydraulic conductivity and pressure head moments. For unsaturated hydraulic conductivity of all

isotropic soils (group A), dimensionless sample errors of mean eqn (10) and variance eqn (11) are found to range from 1.0 to 1.2, indicating that the spatial sample variability of the MCS is in good agreement with the theoretical variability eqns (6) and (9) expected for a Gaussian sampling process, even under highly heterogeneous conditions (Table 2). At anisotropic soil sites,  $\epsilon'_m$  of  $y$  reduces to values between 0.7 and 0.9, while  $\epsilon'_v$  of  $y$  increases in more variable, anisotropic soils to values of up to 1.3. This is attributed to the decrease in domain size relative to the horizontal correlation scale of  $y$ . In the anisotropic soils, the horizontal element size is  $0.1 \lambda_{fx}$  yielding a relative horizontal domain size of  $6.4 \lambda_{fx}$ , while isotropic soils are discretized to  $0.2 \lambda_{fx}$  yielding a relative horizontal domain size  $12.8 \lambda_{fx}$  (see Table 1). The larger the relative domain size, the larger the number of statistically independent samples, which reduces the sampling error relative to the expected variabilities  $\epsilon'_m$  and  $\epsilon'_v$  in an infinite domain. To test this hypothesis, simulations of group A and B are repeated for a soil domain that is four times larger (128 times 128 elements). For such simulation conditions we find that the dimensionless sample errors of the mean and variance converge to values between 0.95 and 1.1.

Head sample mean and sample variance errors  $\epsilon'_m$  and  $\epsilon'_v$  at isotropic soil sites are between 0.6 and 0.7, and between 1.0 and 1.1, respectively (Table 2). In anisotropic soils,  $\epsilon'_m$  of  $h$  ranges from as low as 0.22 (C1,  $\sigma_y^2 = 0.53$ ) to 0.46 (e.g. C3,  $\sigma_y^2 = 3.1$ ). Error  $\epsilon'_v$  of  $h$  increases to as much as 1.4 in strongly variable anisotropic soils, meaning that the actual variance sample error may be as much as 40% larger than estimated by eqn (10). The relatively low values for  $\epsilon'_m$  and high values for  $\epsilon'_v$  are again due to the small domain size relative to the correlation scale of the head. In the anisotropic soils the domain size is only about  $3\lambda_{hx}$  times  $5\lambda_{hz}$ . Dimensionless mean and variance sample errors converge to values between 1.0 and 1.2 in a simulation domain with 128 times 128 elements.

### 3.3 Darcy velocity moments

Spatial variability of local mean flux is comparable to the expected sample errors (Table 2). Sample error  $\epsilon'_m$  is between 0.8 and 1.2 in isotropic soils and between 0.7 and

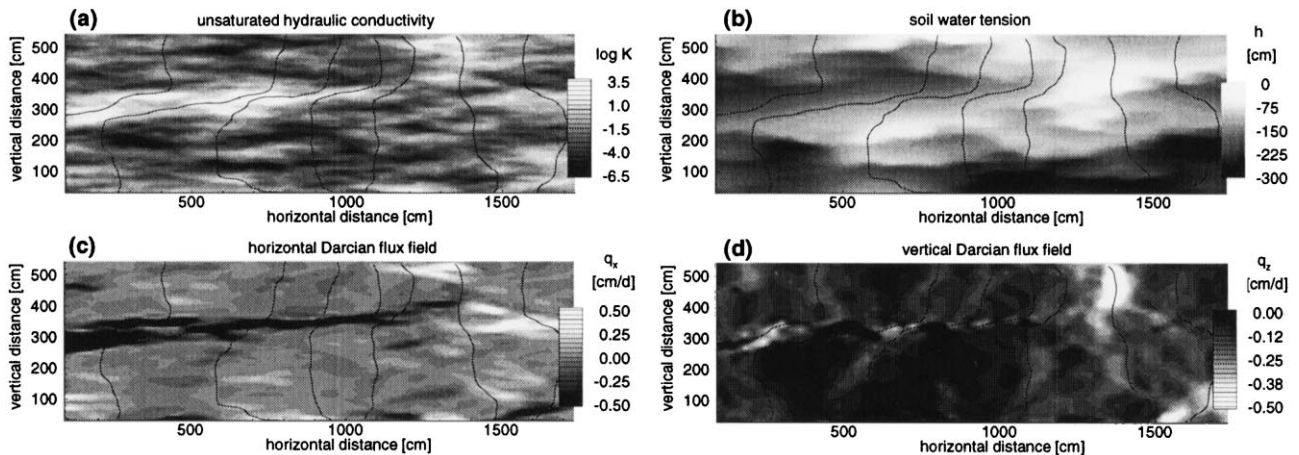


**Fig. 2.** Example realization of a highly variable anisotropic soil (soil B3): (a) unsaturated hydraulic conductivity; (b) soil water tension; (c) horizontal Darcian flux; and (d) vertical Darcian flux. Positive flux is vertically upward and horizontally to the right. Notice that largest absolute values of horizontal flux (white and black areas) occur at or near locations, where vertical flux is also relatively large (white areas). For reference, each panel shows the same set of streamlines computed from the flux fields in (c) and (d).

1.1 in anisotropic soils. In contrast,  $\epsilon'_v$ , in all but the least variable soils, is significantly larger than values expected for Gaussian RSFs. It ranges from 0.9 and 1.1 in mildly heterogeneous soils A1 and A2 to values over 4 in the most heterogeneous soils. Increased simulation domain size decreases dimensionless variance sample errors, yet they are still much larger than 1. The deviation from Gaussian behavior is attributed to the non-Gaussian probability distribution of the Darcian velocity fields, which is further discussed in the next two sections. Local sample mean and variance of the Darcian velocity should therefore be considered to have larger sampling errors than predicted from statistical theory.

### 3.4 Accuracy of average sample moments

In the ensuing analysis, a much higher sampling accuracy is achieved by averaging local sample velocity moments across the simulation domain. We found that the initial first-order perturbation solution as random head boundary adversely affects the results within at most one or two correlation scales,  $\lambda_f$ , from the boundaries. This is similar to the spatial nonstationarity effect of constant head or constant flux boundaries. For the purpose of this study, local sample means and sample variances are, therefore, averaged only across the stationary region of each simulation to further decrease the sampling errors determined above. To determine the 95% confidence interval of the average sample mean and average sample variance, we conservatively assume that there are five statistically independent local sample moments in each dimension of the simulation domain, or approximately one per two correlation lengths. Thus, the sample size  $N \approx 1000$  times  $5^2$ . Using eqn (9) the 95% confidence interval for the sample variance can be shown to be approximately  $\pm 2\%$ . Taking into consideration numerical accuracy, we conclude that for purposes of the following analysis differences between analytically and

numerically determined first and second moments in excess of 4% should be considered significant.

## 4 PHYSICAL OBSERVATIONS OF FLOW IN A RANDOM SOIL: EXAMPLE

To help interpret the MCS results and to discuss and emphasize the direct relationship between stochastic analysis and the physical dynamics of water flow in a heterogeneous soil, we first demonstrate and discuss typical patterns of the various RSFs under investigation using a single realization. The example chosen is an anisotropic soil (soil B3) with a high degree of spatial variability,  $\sigma_y^2 = 3.2$ . The nonlinear solution of  $y$  [Fig. 2(a)] in this relatively wet soil is primarily determined by and, therefore, similar to the saturated hydraulic conductivity distribution. Note that the spatial pattern of unsaturated hydraulic conductivity will converge to that of the saturated hydraulic conductivity as the scaled mean soil–water tension  $\Gamma H$  approaches 0, i.e. the soil becomes saturated. At a given negative value of  $\Gamma H$  (unsaturated flow), the degree of similarity between unsaturated and saturated hydraulic conductivity depends on the correlation between the perturbations of  $a$  and  $f$ , and the variability of  $a$ . In a soil with negligible correlation between  $a$  and  $f$  ( $\rho \approx 0$ ), such as the example shown here, higher variability in  $a$  leads to more variability in unsaturated hydraulic conductivity and less resemblance to the spatial distribution of the saturated hydraulic conductivity field. In the hypothetical case of a soil with perfectly correlated  $a$  and  $f$  properties ( $\rho = 1$ ), the variability of the unsaturated hydraulic conductivity can be shown to disappear at  $\Gamma H_c = -1/\xi$  [see eqn (16)]. At even lower mean soil water tension, variability of unsaturated hydraulic conductivity increases monotonically. The critical pressure,  $H_c$ , separates a wetter unsaturated flow regime that takes place in predominantly coarse textured portions of the soil domain from a drier

unsaturated flow regime that involves fine textured materials in a soil.

The pressure head,  $h$  [Fig. 2(b)] is significantly smoother than the random realizations of  $f$ ,  $a$  or  $y$ . Also, it is more anisotropic than  $y$  with significantly larger spatial continuity in the horizontal direction than in the vertical direction. Vertically, abrupt pressure changes occur at the interface between fine textured soil (indicated by small  $y$ ) and coarse textured soil below (indicated by large  $y$ ). The pressure head in the fine textured soil is higher (less negative) than in the coarse textured soil creating a steep vertical pressure gradient in response to the low hydraulic conductivity in the fine textured soil. Gradients of head,  $h$ , together with gravity are the driving force of unsaturated flow and, therefore,  $h$  tends to equilibrate horizontally across a scale larger than the horizontal scale of soil textural heterogeneities. Stronger continuity in horizontal direction is due to the effects of gravity: Differences in soil water pressure in the horizontal direction are equilibrated by the flow system through adjustment of vertical flux rates at a horizontal scale similar to that of hydraulic conductivity, i.e. a significantly shorter scale than that of the pressure head. The corresponding  $q_x$  and  $q_z$  fields are shown in Fig. 2(c,d). Elongated linear patterns, which are positive and negative diagonal for the transverse component and vertically braided for the longitudinal component, are distinctly different from the random patterns of  $\log K_s$ ,  $\log K$ , or pressure head realizations. Horizontal and vertical flux realizations are complimentary, mutually dependent components of the flux vector  $\mathbf{q}$ . We observe that very large horizontal flux occurs only where vertical flux is also large and where the overall flux direction is at an angle to the vertical axis. Locations with a large horizontal flux component connect non-vertically aligned locations of high vertical flux. Together, these high flux channels define a continuous network of braided preferential flow parts. In contrast, large parts of the remaining soil domain contribute relatively little to moisture flux. Accumulation of moisture flux into narrow channels increases with soil textural heterogeneity. It also increases with soil dryness. Both cause an increase in unsaturated hydraulic conductivity variance. Similar patterns of flow channeling were shown by Moreno et al.<sup>34</sup> who modeled saturated Darcy flow in a two-dimensional, single fracture with varying aperture and high variability of fracture resistance (which is inversely related to the conductivity). Moreno and Tsang<sup>35</sup> demonstrated that channeling effects in saturated three-dimensional porous media are very pronounced, when hydraulic conductivity variance is large. Preferential flow has also been observed in field soils, where channeling due to soil heterogeneity and wetting front instability (fingering) may greatly enhance the variability of the flux field<sup>16</sup>.

The qualitative features of soil hydraulic properties are consistent with those described in other analyses of soil water flux dynamics through simulated cross-sections of hypothetical heterogeneous soils<sup>1,38,41,43</sup>. In particular, a good qualitative agreement is obtained between the example

in Fig. 2, which is based on Gardner<sup>14</sup> parametrization of  $K$ , and simulations based on self-similarity and Van Genuchten<sup>47</sup> parametrization<sup>41</sup>. The agreement can be explained by comparing the nature of the unsaturated hydraulic conductivity function in that particular example. Within the narrow range of soil water tension observed in the Van Genuchten soil<sup>41</sup>, unsaturated hydraulic conductivity functions are approximately log-linearly dependent on head. Under those circumstances, the realizations of self-similar, Van Genuchten soils corresponds to Gardner soils with  $f$  and  $a$  being perfectly correlated. Also note that Roth<sup>41</sup> has demonstrated that the particular choice of covariance function for  $f$  and  $a$  has minor impacts on the global structure of the unsaturated flow field, suggesting that the analysis provided here has implications that are, at least qualitatively, not limited to the particular random field or hydraulic models chosen in this analysis. We will demonstrate next, that important aspects of soil dynamics qualitatively described here and in studies such as Roth<sup>41</sup> have a well-founded mathematical-stochastic basis and can to a limited degree of accuracy be predicted by existing analytical stochastic models.

## 5 NUMERICAL STOCHASTIC ANALYSIS AND VALIDATION OF ANALYTICAL MODEL

### 5.1 Sample probability distribution function (PDF)

Marginal sample probability distribution functions of the individual RSFs were sampled from over 300 discrete histogram classes and are therefore shown as continuous distributions. Fig. 3 shows a typical example of a soil with moderate heterogeneity (soil A3). The probability plots of  $y$  and  $h$  at all soil sites indicate that these RSFs are Gaussian-like distributed [e.g. Fig. 3(a,b)]. These findings confirm assumptions about the distribution of  $y$  and  $h$  in the analytical work by Yeh et al.<sup>53–55</sup> and Mantoglou et al.<sup>29–31</sup>. Deviations from Gaussian distributions, particularly in soils with large variability of  $y$ , occur at the tails of the cumulative distributions, particularly those of  $h$ .

Sample distributions for the longitudinal component  $q_z$  are found to be approximately lognormal [Fig. 2(c)]. Formal testing for lognormal distribution by the  $\chi^2$  and Kolmogorov–Smirnov method<sup>20</sup> was negative at the 1% level due to significant differences between sample distributions and lognormal distribution near the tail ends, particularly for small  $q_z$ . By heuristic argument,  $q_z$  cannot be lognormally distributed, because zero  $q_z$  or even upward  $q_z$  are physically possible as demonstrated in Fig. 2(d). Note that sample distributions similar to those from the complete RSF sampling set are obtained from the limited data set obtained at the domain center point only [black dots in Fig. 3(c)]. The agreement between the exhaustive sample distribution and the single sample point distribution rules out that the shape of the sample distribution is due to non-stationarity within the sample domain. The results are in

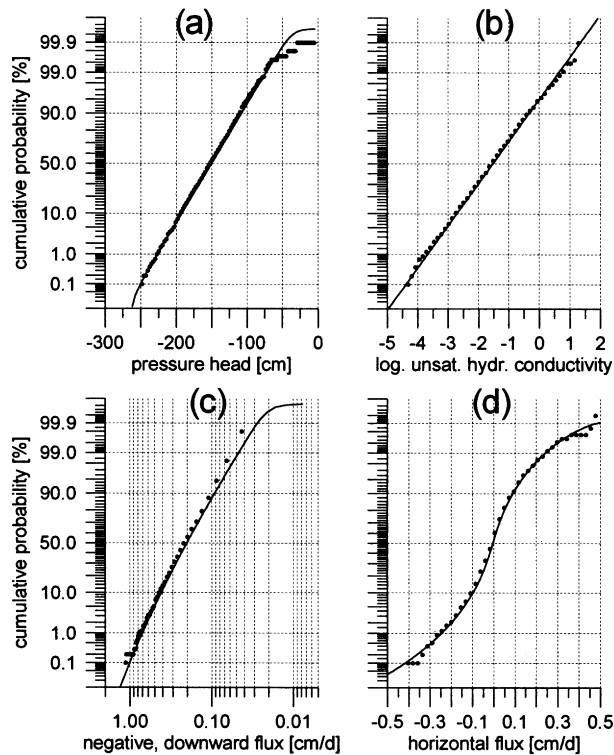


**Fig. 3.** Sample probability distributions of (a)  $h$ ; (b)  $y = \ln K$ ; (c)  $q_z$ ; and (d)  $q_x$  from 1000 realizations of the isotropic reference soil. The solid line represents the total sample (all points in each realization) of more than 4 million sampling points. The solid circles represent a sample of 1000 head values taken at sample point 5 (see Fig. 1).

accordance with the longitudinal flux distributions obtained from Monte Carlo simulations of saturated flow in two- and three-dimensional heterogeneous media by Bellin et al.<sup>4</sup> and with unsaturated flow results for a two-dimensional, Miller-similar medium<sup>41</sup>.

Horizontal flux probability distributions of all soils are symmetric, but strongly leptokurtic. For the isotropic soil A3, for example, the kurtosis is 7.25 [Fig. 3(d)]. This empirically determined form of the transverse flux distribution is at first glance in contrast to the findings of Bellin et al.<sup>4</sup> who reported that the horizontal flux component in their simulations of strongly heterogeneous saturated porous media has a normal pdf. However, visual inspection of Figure 7(d) in Bellin et al.<sup>4</sup> indicates that their corresponding transverse velocity pdf qualitatively also tends to be leptokurtic. The leptokurtic form of the horizontal flux pdf and the skewed distributions of the vertical flux pdf are consistent with the observation of preferential flow in the example presented above. Under heterogeneous flow conditions the magnitude of  $q_x$  is most likely small or even zero, but in the preferential flow areas, which are by definition of limited spatial extent,  $q_x$  is likely to be very large in either positive or negative direction, while  $q_z$  is large only in vertically downward direction. Hence the long tail on either end of the pdf of  $q_x$ , but only on one end of the pdf of  $q_z$  giving the latter the impression of a quasi-lognormal

distribution. Because large positive or negative transverse flux conditions are likely to be associated with large longitudinal (vertical) flux conditions, in particular under isotropic conditions, it is not surprising that the pdfs of the two flux components are not found to be completely independent. Note that on the other hand, small transverse flux values are not strongly correlated with longitudinal flux values.

These findings have important implications on our understanding of solute flux. In contrast to our numerical results, analytical stochastic transport models<sup>13,15</sup> assume that the two flux components are statistically independent and Gaussian distributed. The correlation between large components of horizontal and vertical flux, the leptokurtic distribution of horizontal flux, and the significant lateral variability of high velocity flow channels explains, why observed transverse spreading of inert solutes in soil water is significantly larger than predicted by analytical transport models<sup>23</sup>.

## 5.2 Analysis and comparison of first moments (mean)

After empirically determining the general form of the probability distribution functions for  $y$ ,  $h$  and  $q$ , the next stochastic property of interest is the first moment of the probability density function of each of these RSFs. The set of simulations performed are compared to analytical models relating the RSF's mean to variability of  $f$  and  $a$ ,  $\sigma_f^2$  and  $\sigma_a^2$ , mean soil water tension prescribed on the boundaries, degree of anisotropy,  $\nu$ , and dimensionless vertical correlation scale of  $f$ ,  $\Gamma\lambda_{fz}$ . These are the soil and infiltration parameters determining the average soil water tension, unsaturated hydraulic conductivity, and soil water flux.

The average sample mean of the log unsaturated hydraulic conductivity,  $Y$ , is found proportional to  $H$  such that for all tested soils the analytical approximation of  $Y$ ,  $Y = F + HT$ , holds accurately: deviations are less than 1%. The deviations of the sample mean head averaged across the simulation domain from the mean head prescribed for the first-order head perturbations on the boundary are less than 0.1% in a relatively homogeneous soil (e.g. soil A1) and less than 1% even if the head variance is very large. These small differences indicate that the numerical mass-balance errors are reasonably small, even for simulations of highly heterogeneous unsaturated flow conditions.

Due to the mean vertical, uniform flux, the mean horizontal flux should vanish. Indeed all simulations render average sample mean horizontal flux,  $Q_x$ , to be at least three orders of magnitude smaller than the mean vertical flux,  $Q_z$ . It is, therefore, considered negligible. The first order analytical mean  $Q_z$  is

$$Q_z = K_m \quad (12)$$

where  $K_m = \exp(Y)$  is the geometric mean of the unsaturated hydraulic conductivity. The first-order analysis assumes that both the vertical and horizontal velocities have a normal distribution. Although the assumption does not hold, the difference between analytically and

**Table 3. Comparison of the numerical and first-order analytical mean of dependent RSFs head  $h$ , unsaturated hydraulic conductivity  $y$ , horizontal velocity  $q_x$ , and vertical velocity  $q_z$ . The examples here are group A (isotropic, wet soils) with  $\sigma_y^2$  ranging from 0.01 to 0.9. Also shown is group B (anisotropic, wet soils) with  $\sigma_y^2$  ranging from 0.7 to 3.1 (see Table 1). Length units are in [m]. Time units are arbitrary**

	A1 MCS	anal.	A2 MCS	anal.	A3 MCS	anal.
$h$ :mean	-1.501	-1.500	-1.504	-1.500	-1.509	-1.500
$y$ :mean	-1.499	-1.500	-1.503	-1.500	-1.498	-1.500
$q_x$ :mean	$-3.18 \times 10^{-7}$	0.00	$-1.03 \times 10^{-6}$	0.00	$-4.35 \times 10^{-6}$	0.00
$q_z$ :mean	$-2.2322 \times 10^{-3}$	$-2.231 \times 10^{-3}$	$-2.230 \times 10^{-3}$	$-2.231 \times 10^{-3}$	$-2.29 \times 10^{-3}$	$-2.231 \times 10^{-3}$
	B1 MCS	anal.	B2 MCS	anal.	B3 MCS	anal.
$h$ :mean	-1.510	-1.500	-1.529	-1.500	-30.06	-30.00
$y$ :mean	-1.507	-1.500	-1.533	-1.500	-30.17	-30.00
$q_x$ :mean	$-9.95 \times 10^{-7}$	0.00000	$3.49 \times 10^{-6}$	0.00000	$-4.56 \times 10^{-18}$	0.00000
$q_z$ :mean	$-1.78 \times 10^{-3}$	$-2.23 \times 10^{-3}$	$-1.39 \times 10^{-3}$	$-2.23 \times 10^{-3}$	$-4.26 \times 10^{-14}$	$-9.36 \times 10^{-14}$

numerically obtained  $Q_z$  in isotropic soils with  $\sigma_f^2 \leq 1$  is insignificant (less than 3%, see Table 2).

In contrast, the simulations show that  $K_m$  is a poor estimator of mean vertical flux in moderately to highly heterogeneous soils, particularly if the soil is anisotropic. In the example of a highly heterogeneous isotropic soil (A4), the simulated sample  $Q_z$  is 10% larger than computed from eqn (12). On the other hand, the average sample  $Q_z$  in the anisotropic, wet soils with  $\sigma_f^2 = 1$ , is more than 20% smaller and decreases in more heterogeneous systems to less than 50% of  $K_m$ . The decrease in the average mean flux relative to the analytical prediction must be explained by the neglect of higher order moments in the derivation of eqn (12), which are significant given the lognormal distribution of  $q_z$  and the preferential flow patterns, particularly in anisotropic soils with  $\sigma_y^2 \geq 1$ . As expected, the numerical results demonstrate that the average steady state flux in highly heterogeneous soils strongly depends on  $\sigma_y^2$  and on the anisotropy ratio.

Because the average gradient in all simulated soil profiles is unity, the mean average soil water flux is by definition equal to the effective hydraulic conductivity,  $K_e$ , of the soil transect, where  $K_e = Q_z / \langle \partial h / \partial z \rangle$ . A mixed higher-order analysis of  $K_e$  was presented by Yeh et al.<sup>54</sup> for soils similar to those presented here, but with normal (instead of log-normal) distributed  $\alpha$ . They demonstrate that, for  $\Gamma \lambda_{fz} < 1$ , and flow normal to soil stratification ( $\nu \gg 1$ ), the effective hydraulic conductivity is smaller than the geometric mean hydraulic conductivity. In the limit, as  $\nu \rightarrow \infty$  (perfectly stratified soil), the effective hydraulic conductivity approaches the harmonic mean,  $K_h$ , of  $y$ , where  $K_h = K_m^* \exp(-\sigma_y^2/2)$ . Based on their analysis, the effective hydraulic conductivity for anisotropic soils with  $\nu = 6$ , for example, is approximately 80% of  $K_m$  for  $\sigma_y^2 = 1$ , and approximately 50% of  $K_m$  for  $\sigma_y^2 = 3$ , which compares well with the mean vertical flux measured in the Monte Carlo simulation.

Overall, the results indicate that existing analytical stochastic models are able to accurately predict average hydraulic conductivity and flow conditions in an unsaturated

soil, even if soil heterogeneity exceeds the limitations assumed in the analytical models. From a practical point of view, the analytical method should be a useful tool to predict the average behavior of the flow in unsaturated zone (Table 3).

### 5.3 Analysis and comparison of second moments (variance)

The second moment of a RSF is a measure of the uncertainty in our ability to predict soil water tension and flux. Accuracy in predicting variability of  $h$ ,  $y$  and  $q$  is important not only to estimate average soil water flux, but to determine the potential uncertainty of solute transport in soils<sup>23</sup>. Here, we analyze the second moments obtained from the Monte Carlo simulation in their dimensionless form. The dimensionless variance of  $y$ ,  $h$ ,  $q_x$  and  $q_z$  are defined by:

$$\sigma_y^2 = \frac{\sigma_y^2}{\sigma^2} \tag{13}$$

$$\sigma_h^2 = \frac{\sigma_h^2}{\sigma^2 \lambda_{fz}^2} \tag{14}$$

$$\sigma_{q_x}^2 = \frac{\sigma_{q_x}^2}{\sigma^2 K_m^2} \tag{15}$$

$$\sigma_{q_z}^2 = \frac{\sigma_{q_z}^2}{\sigma^2 K_m^2}$$

where  $\lambda_{fz}$  is the vertical correlation scale of  $f$ . The variance factor  $\sigma^2$  is given by:

$$\sigma^2 = \sigma_f^2 [1 + 2\rho\zeta\Gamma H + (\zeta\Gamma H)^2] \tag{16}$$

where  $\zeta = \sigma_a / \sigma_f$ . The four dimensionless variances are plotted as functions of four independent variables: soil variability,  $\sigma_f^2$ , mean soil water tension,  $H$ , anisotropy ratio,  $\nu$  and dimensionless vertical correlation scale,  $\Gamma \lambda_{fz}$ . Results are shown in a  $4 \times 4$  matrix diagram (Fig. 4).

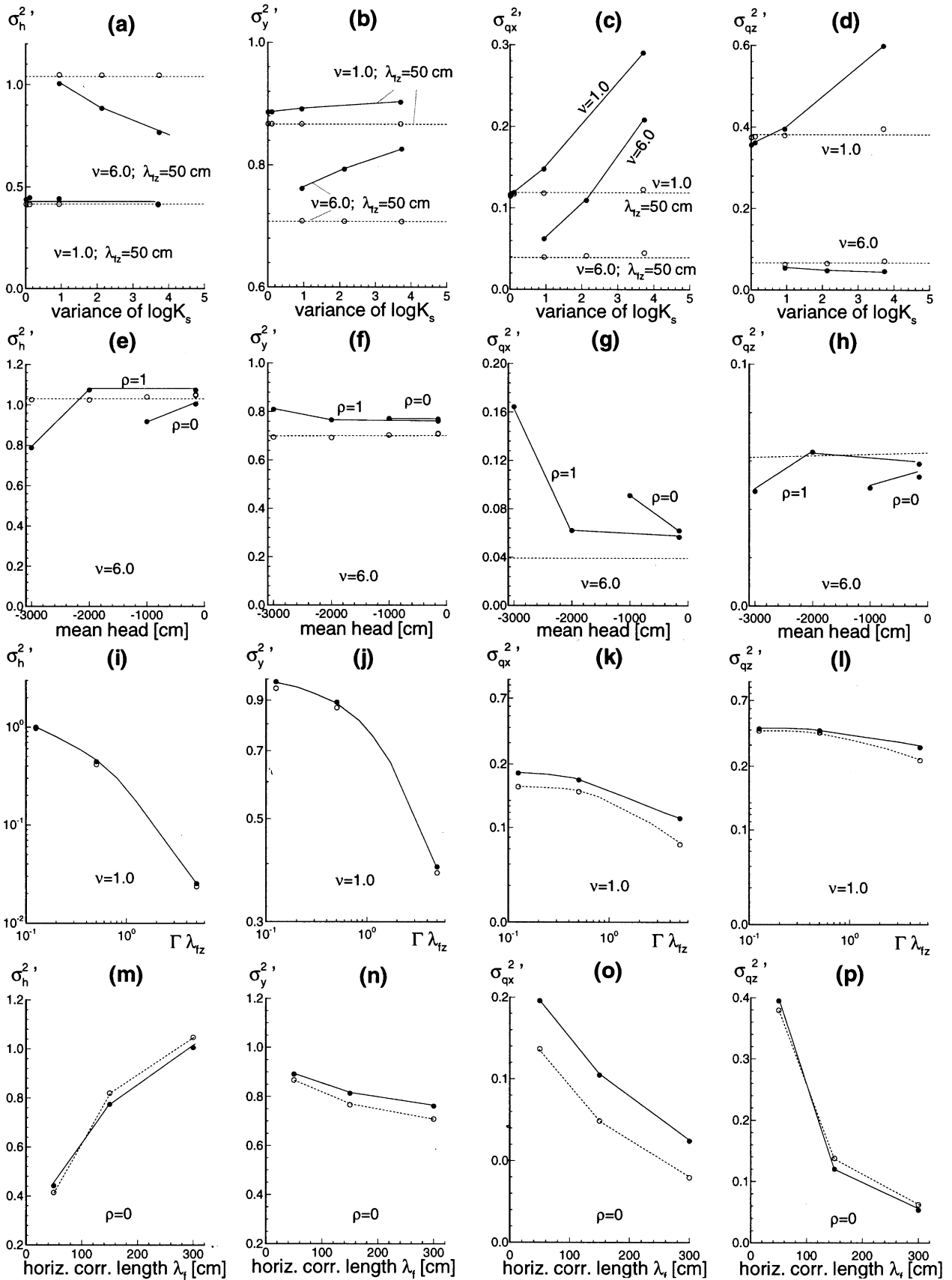


**Fig. 4.** (From left to right:) Variance of head, unsaturated hydraulic conductivity, horizontal flux, and vertical flux as functions of (from top to bottom:) soil textural variability (indicated by  $\sigma_s^2$ ), mean soil water tension, dimensionless vertical correlation scale, and anisotropy ratio. Dashed lines with hollow symbols represent spectral analytical solutions. Solid lines with black symbols are measured by MCS. Note that results are shown by soil group: soil groups A and B are shown in figures (a)–(d), soil groups C and D are shown in figures (e)–(h), soil group E is shown in figures (i)–(l), and soil group F is shown in figures (m)–(p).

In soils with small variability, dimensionless variances  $\sigma_y'^2$ ,  $\sigma_h'^2$ ,  $\sigma_{q_x}'^2$ , and  $\sigma_{q_z}'^2$  are independent of  $\sigma_f^2$ ,  $\rho$ ,  $\zeta$  and  $H$ , according to the analytical model and as demonstrated by the Monte Carlo results [Fig. 4(a–d)]. An exception is the horizontal flux variance, which agrees with the analytically approximated results only in the least variable example soil, where  $\sigma_f^2 = 0.01$ . MCS results of horizontal flux variance exceed the analytical model by more than 40% at  $\sigma_f^2 = 1$ . Differences reflect the leptokurtic distribution of the horizontal flux and the neglect of higher order moments in the analytical model.

Significant deviations of the analytical solution from almost all the MCS simulated variances of  $y$ ,  $h$  and  $q$  are observed in highly variable soils with  $\sigma_f^2 \geq 1$ . Simulated variances of head are significantly lower than predicted by the analytical model while the variability of  $y$  and  $q$  is higher than predicted. Differences increase with  $\sigma_f^2$  and are as much as 10% for the variance of  $y$ , 25% for the variance of  $h$ , 50% for the variance of  $q_z$  and 500% for the variance of  $q_x$  [Fig. 4(a–d)].

Notably, the simulated variance of vertical flux in anisotropic soils [Fig. 4(d)] is smaller (not larger) than predicted by the analytical model with differences of as much as 30%. This may be the result of the fact that the absolute value of the vertical flux is significantly smaller than estimated by the first-order analytical model. Average vertical flux in the most heterogeneous, anisotropic soil example is less than 50% of the first-order estimate eqn (12). Hence, the coefficient of variation, which measures variability relative to the average value, is up to 70% larger in the Monte Carlo simulation than the coefficient of variation predicted from first-order analysis.

High variability of  $y$  and, therefore, high variability of flux may be observed not only in texturally heterogeneous soils (large  $\sigma_f^2$ ), but also in relatively homogeneous soils under dry flux conditions because of the dependency of  $\sigma_y^2$  on mean soil water tension,  $H$ . This is consistent with the analytical model, which predicts that variability of  $y$ ,  $h$  and  $q$  is proportional to  $\sigma^2$ , defined in eqn (16), but not only do the MCSs show higher variability in drier soils. Also, the shortcomings of the analytical model with respect to the numerical results for dry soils of moderate textural variability ( $\sigma_f^2 = 1$ ) are similar to those for the wet texturally very variable soils [compare results at  $H = -30$  m in Fig. 4(e–h) to those at  $\sigma_f^2 = 4$  in Fig. 4(a–d)]. In both cases, the unsaturated hydraulic conductivity is large ( $\sigma_y^2 \gg 1$ ). Like saturated hydraulic conductivity variance in aquifer flow, unsaturated hydraulic conductivity variance is the key variable in determining the variability of soil water tension, soil water flux, and ultimately solute transport in the vadose zone. The Monte Carlo simulations demonstrate that the accuracy of the analytical stochastic model is not a function of soil variability (determined by  $\sigma_f^2$  and  $\sigma_a^2$ ) alone. It is also a function of soil water tension or soil moisture content. Dry soils, whether texturally more or less heterogeneous, are dominated by highly heterogeneous flux conditions, for which analytical stochastic models are necessarily of

limited applicability. Analysis and prediction of moisture flux and transport of environmental tracers (e.g. natural isotopes) in deep soils of arid climate regions is, therefore, more accurately represented by numerical stochastic methods. Nonetheless, for practical applications where high accuracy (in the statistical sense) is not a requirement, analytical methods may give excellent preliminary results without the expense of time-consuming numerical simulations.

Note that the unsaturated hydraulic conductivity variance as a function of mean pressure head varies fundamentally different in a soil with  $\rho = 1$  when compared to soils with  $\rho = 0$ . In soils with uncorrelated  $f$  and  $a$ , differences between analytical and numerical stochastic solution increase as drier soil conditions are investigated due to increasing  $\sigma_y^2$ . In soils with perfectly correlated  $f$  and  $a$ , on the other hand, the variance of  $y$  first decreases as mean soil water tension increases. This explains, why the analytical stochastic results for the variance of  $y$ ,  $h$  and  $q$  are valid for much drier soils if  $\rho = 1$ , than for soils where  $\rho = 0$ . For soils with  $\rho = 1$ , the critical soil water pressure is at  $H = -10$  m and as shown in Fig. 4(e), differences between analytical and numerical head variance are not significant at  $H \geq -20$  m. In a much drier, albeit only moderately heterogeneous soil (soil C3,  $H = -30$  m), the RSF variances and their deviations from the analytical model are similar to those in the wet, highly heterogeneous soil B3.

Changes in anisotropy ratio [Fig. 4(i–l)] and in the dimensionless vertical correlation scale  $\Gamma\lambda_{fz}$  [Fig. 4(m–p)] have apparently no significant effect on the accuracy of the analytically determined variances of  $y$  and  $h$ . Only simulated flux variances increase significantly at large  $\Gamma\lambda_{fz}$ , even if  $\sigma_f^2$  remains constant. The increased variability of flux may be due to the increased nonlinearity of the governing flow equation caused by a tenfold increase in  $\Gamma$ . The increase in  $\Gamma$  (coarser soil texture) is associated with a significant reduction of the average pore scale length,  $\Gamma^{-1}$ . Changes in soil water tension may, therefore, occur over much shorter distances, creating larger head gradients and, therefore, an increase in flux variance. The analytical model apparently does not account for the effect of increased nonlinearity, due to the linearization implicit to the analytical results.

#### 5.4 Comparison of correlation and cross-correlation functions

Correlation functions are a measure of the spatial persistence and continuity of a RSF. Spatial continuity varies with direction, often along principal coordinates. In some cases, the direction of largest continuity, however, does not coincide with the principal coordinate axis. For example, the direction of major continuity of  $q_x$  is diagonal to the principal flow axes. Therefore, the major axes of the multi-dimensional correlation function of  $q_x$  would also be diagonal. Correlograms or variograms along the principal coordinates, the standard tools in most empirical stochastic analyses of flow processes, are therefore of limited value, particularly for the analysis of soil water flux components

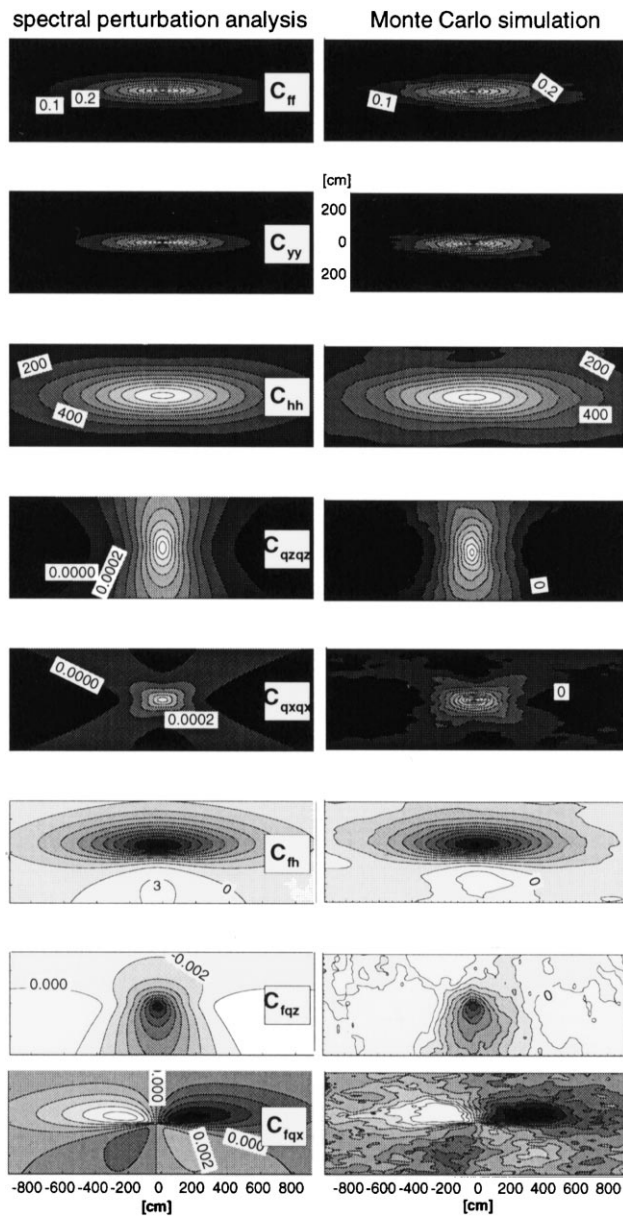


**Fig. 5.** Comparison of analytical (left) and MCS (right) covariance and cross-covariance functions for an anisotropic soil (B1). The shown MCS (cross-)covariances are obtained for sample point 5 (see Fig. 1) and based on 1000 sample realization. From top to bottom: covariances of saturated hydraulic conductivity,  $f$ , unsaturated hydraulic conductivity,  $y$ , soil water tension,  $h$ , vertical flux,  $q_z$ , and horizontal flux,  $q_x$ ; cross-covariances between  $f$  and  $h$ , between  $f$  and  $q_z$ , and between  $f$  and  $q_x$ . The  $x$ -axes show horizontal lag-distances, the  $y$ -axes vertical lag-distances. contour intervals and shading are identical for analytical and MCS results. All units of length in [cm].

(Fig. 2). The same argument holds for cross-correlation functions, which often have multiple maxima and minima and may not be symmetric (as opposed to correlation functions of stationary RSFs, which, by definition, have a single maximum at the origin and are symmetric with respect of the origin). Here, we analyze the complete two-dimensional correlation and cross-correlation field.

Fig. 5 demonstrates that empirically obtained local (non-averaged) correlation and cross-correlation fields of  $y$  and  $h$  are in excellent agreement with the theoretical correlation functions derived from spectral analysis and reflect the general patterns of unsaturated hydraulic conductivity and soil water tension distribution found in a hypothetical soil cross-section such as the one discussed above. For reference, the exponential input covariance function of  $f$ ,  $C_{ff}$ , is also shown. The correlation scales of  $C_{hh}$  are much larger than those of  $C_{yy}$  and are anisotropic even if the hydraulic conductivity structure is isotropic, i.e. nonlayered. The head covariance function reflects the strong spatial continuity, particularly in the horizontal direction, observed in the random soil of Fig. 2. Overall qualitative agreement between analytical and MCS solutions, particularly with respect to spatial structure, is found at all sites. For better quantitative comparison, we use vertical and horizontal cross-sections of the (normalized) correlation functions  $\rho_{ff}$ ,  $\rho_{yy}$ ,  $\rho_{hh}$ . Examples of correlation functions of both, a mildly and strongly heterogeneous soil (C1 and C3) are plotted in Fig. 6. As expected, analytical and numerical correlation functions for  $f$  are identical. Similar agreement is found for  $\rho_{yy}$  in all soils. Only in strongly heterogeneous soils, the scale of the analytical head correlation function tends to underestimate the head correlation scale determined from the Monte Carlo results. The similarity of  $\rho_{yy}$  or  $\rho_{hh}$  (e.g. Fig. 6) with results by Roth<sup>41</sup> indicate that the spectral method can be a powerful tool to also approximate stochastic analysis of flow in isotropic, Miller-similar media soil with Van Genuchten parametrization.

Covariance fields for  $q_x$  reflect the diagonal patterns, which are observed in individual flux realizations discussed earlier. Covariance of  $q_x$  is strongest in the diagonal directions (relative to mean flow direction) and very small in vertically overlying or horizontally adjacent location, i.e. in the vertical or horizontal direction. On the other hand, the covariance function of  $q_z$  is highly anisotropic with the major anisotropy axis in mean flow direction. This is not surprising considering the strong vertical continuity and the relative small lateral extent of the preferential flow channels described above. Cross-sections of the normalized covariance and cross-covariance functions show that analytical flux correlation functions deviate significantly from numerically determined solutions, if  $\sigma_y^2 > 1$ . This applies again to both, wet, texturally very heterogeneous soils (e.g. B3) and dry, texturally rather homogeneous soils (e.g. C3, Fig. 6). Vertical flux correlation functions in the MCS have a shorter longitudinal correlation scale than analytical correlation functions. The transverse hole-type correlation of  $q_z$  is accurately predicted by spectral first-order analysis, while the analytical model significantly underestimates the horizontal correlation scale of  $q_x$  when the flux is highly variable (Fig. 6).

The good agreement between analytically predicted and numerically derived cross-covariance fields (Fig. 5) is of practical importance for the estimation of cross-covariances. Such agreement allows stochastic modelers

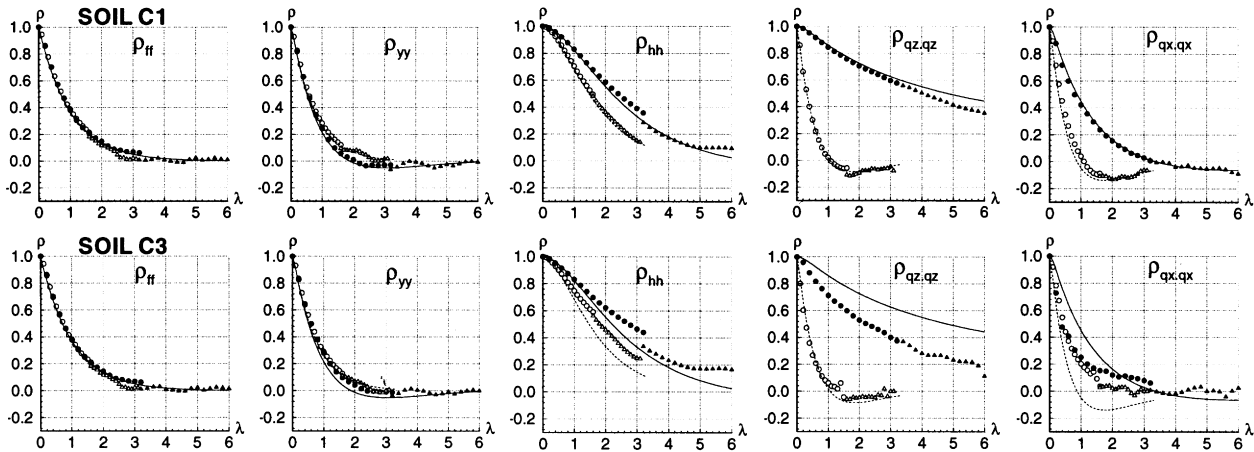


**Fig. 6.** Vertical (solid lines and black symbols) and horizontal (dashed line and white symbols) cross-sections of the correlation functions  $\rho_{ff}$ ,  $\rho_{aa}$ ,  $\rho_{hh}$ ,  $\rho_{qz}$ ,  $q_z$  and  $\rho_{qx,qx}$ . Lines are from the spectral analysis, while symbols are results from MCS. Circles represent the average of the eight correlation functions at sample point 1 through 9. Triangles are from the sample correlation functions at sample point 5, which has a larger window and therefore gives values at larger lag-distances (Fig. 1). The vertical and horizontal correlations are plotted as functions of vertical and horizontal correlation scales for  $f$ , respectively. The two examples are for soil C1 (top) and C3 (bottom).

to determine cross-covariance functions analytically and calibrate their magnitude by Monte Carlo simulation or field measurements. The ability to provide calibrated analytical cross-covariance functions is an important step for solving a number of stochastic problems<sup>10–12,29,30,42,53,54</sup>. Cross-covariances are also necessary for the implementation of conditional simulation<sup>24</sup> and geostatistical inverse modeling<sup>58</sup>. The Monte Carlo technique coupled with analytical tools, therefore, presents an opportunity to avoid the empirical determination of non-symmetric cross-covariances from field data, which would be difficult, if not impossible.

## 6 SUMMARY

Monte Carlo simulations of steady-state flow under gravity drainage conditions in a deep, heterogeneous vadose zone have been implemented:

- to provide exact results for the stochastic boundary value problem approximated by existing analytical models;
- to rigorously assess the accuracy of first-order analytical stochastic methods for a wide range of soil conditions;
- to demonstrate the link between stochastic theory<sup>29–31,53–55</sup> and empirical, numerical and field results<sup>1,26,38,41,43,51</sup> reflecting other, more realistic, but also more complex, scenarios.

We present a comprehensive validation of existing analytical stochastic models of unsaturated, steady state flow by developing and implementing an accurate numerical stochastic analysis that allows us to investigate a large range of soil conditions, particularly regarding a realistic range of highly variable soil water flux conditions. To validate the

numerical approach, we show that sampling errors associated with Monte Carlo simulation are in reasonable agreement with theoretical Gaussian sampling errors and can, therefore, be predicted a priori. In our simulations, we achieve a high confidence limit (sample error variance of less than 2% for both first and second moment) by averaging stationary local sample moments over the simulation domain. By the same token this study underlines the need for using a large number of realizations in Monte Carlo simulations, particularly if nonstationary conditions are simulated where spatial averaging of local sample moments is not possible.

In agreement with previous research, the Monte Carlo analysis demonstrates that the analytical first-order perturbation solutions for mean and variance of the dependent RSFs,  $y$ ,  $h$  and  $q$ , are in good agreement with numerical solutions if the variance of  $y$ , a dependent parameter, is less than 1 (mildly to moderately variable flow). Two-dimensional covariance and cross-covariance functions are also in good agreement with numerically sampled (cross-)covariance fields. For  $\sigma_y^2 \geq 1$  (moderate to strong variable flow) spectral analysis of first-order moments provides general insights, but the actual, fully nonlinear MCS solutions for various dependent moments differ significantly from the analytical predictions. In particular, flux variability is strongly underestimated by the analytical model due to the highly skewed probability distribution of longitudinal flux. The probability distribution of vertical flux is approximately log-normal, while horizontal flux is characterized by a leptokurtic distribution. The probability distributions of horizontal and vertical flux are not statistically independent. The skewed, dependent probability distributions reflect the preferential flow patterns found in individual realizations of soil water flux. Differences between analytical and numerical model are explained by the fact that the

linearized Gaussian analysis does not account for such highly nonlinear occurrence of preferential flow.

In agreement with analytical models, numerically determined variances for  $h$ ,  $y$ ,  $q_x$  and  $q_z$  in wet, texturally heterogeneous soils are found to be similar to those in dry, texturally almost homogeneous soils with high variability of unsaturated hydraulic conductivity. The disparity between numerical and analytical results for soils with high textural variability is shown to be similar to that found for relatively homogeneous soils under dry flow conditions. In both cases,  $\sigma_y^2$  is large. It is, therefore, important to recognize that the application of analytical stochastic models to relatively homogeneous soils does not automatically imply accuracy of first-order approximations. Rather, the analytical spectral model gives accurate results only if the soil with  $\sigma_f^2 < 1$  is relatively wet, i.e. soil water flux and not just texture is relatively homogeneous.

On a more practical side, where accuracy is often measured in orders of magnitude rather than in percent, we are encouraged to find that for the large range of soil texture and soil flux conditions, analytical stochastic models are within a factor 2 of the actual moments. For many engineering problems, the application of the analytical model seems therefore justified, even if flow is highly variable. Other factors, not included in the simplified conceptual model underlying both the numerical and analytical methods presented here, may contribute more to estimation errors than the differences observed between nonlinear numerical analysis and analytical results. In applications of Monte Carlo simulations to real world sites, spatially variable soil moisture content, transient flux conditions near the land surface<sup>43</sup>, nonstationary conditions with spatially variable mean head (dictated by boundary conditions)<sup>26,33</sup>, the inclusion of local hysteretic effects<sup>33</sup>, and the use of realistic parametrization of the hydraulic conductivity and soil water retention function<sup>41,47</sup> are important features that are not accounted for by current analytical models. Yet, results presented here show encouraging qualitative agreement with many of those findings indicating that stochastic unsaturated flow theory is capable of capturing many of the fundamental principles of variably saturated flow described in both field experiments and empirical computational experiments despite the underlying simplifying assumptions.

## ACKNOWLEDGEMENTS

This work was funded in part by DOE grant DE-FG02-91-ER61199, the United States Geological Survey, contract #14-08-0001-G2090, and the United States Environmental Protection Agency, contract #R-813899-01-1. We would also like to thank the anonymous reviewers for their many helpful comments.

## REFERENCES

1. Ababou, R., Three-dimensional flow in random porous media. Ph.D. thesis, Department of Civil Engineering, Massachusetts Institute of Technology, Cambridge, MA, 1988.
2. Anderson, S. H. and Cassel, D. K. Statistical and autoregressive analysis of soil physical properties of Portsmouth sandy loam. *Soil Sci. Soc. Am. J.*, 1986, **49**, 1096–1104.
3. Bakr, A. A., Gelhar, L. W., Gutjahr, A. L. and McMillan, J. R. Stochastic analysis of the effect of spatial variability in subsurface flows, 1: comparison of one- and three-dimensional flows. *Water Resour. Res.*, 1978, **14**, 263–271.
4. Bellin, A., Salandin, P. and Rinaldo, A. Simulation of dispersion in heterogeneous porous formations: statistics, first-order theories, convergence of computations. *Water Resour. Res.*, 1992, **28**, 2211–2227.
5. Brigham, E. O., *The Fast Fourier Transform and its Applications*. Englewood Cliffs, N.J., 1988.
6. Ciollaro, G. and Comegna, V. Spatial variability of soil hydraulic properties of a psammic palexeralf soil of South Italy. *Acta Horticulturae, Int. Soc. for Horticultural Science*, 1988, **228**, 61–71.
7. Crosby, J. W., Johnstone, D. L., Drake, C. H. and Renston, R. L. Migration of pollutants in a glacial outwash environment, 1. *Water Resour. Res.*, 1968, **4**, 1095–1113.
8. Crosby, J. W., Johnstone, D. L., Drake, C. H. and Renston, R. L. Migration of pollutants in a glacial outwash environment, 2. *Water Resour. Res.*, 1971, **7**, 204–208.
9. Crosby, J. W., Johnstone, D. L., Drake, C. H. and Renston, R. L. Migration of pollutants in a glacial outwash environment, 3. *Water Resour. Res.*, 1971, **7**, 713–720.
10. Cvetkovic, V., Shapiro, A. M. and Dagan, G. A solute flux approach to transport in heterogeneous formations, 2. Uncertainty analysis. *Water Resour. Res.*, 1992, **28**, 1377–1388.
11. Dagan, G. Solute transport in heterogeneous porous formations. *J. Fluid Mechanics*, 1984, **145**, 151–177.
12. Dagan, G. Theory of solute transport by groundwater. *Ann. Rev. Fluid Mech.*, 1987, **19**, 183–215.
13. Dagan, G., *Flow and Transport in Porous Formations*. Springer, Berlin, 1989, 485 pp.
14. Gardner, W. R. Some steady state solutions of unsaturated moisture flow equations with applications to evaporate from a water table. *Soil Sci.*, 1958, **85**, 228–232.
15. Gelhar, L. W., *Stochastic Subsurface Hydrology*. Prentice-Hall, Englewood Cliffs, N.J., 1993, 390 pp.
16. Glass, R. J., Steenhuis, T. S. and Parlange, J.-Y. Wetting front instability as a rapid and far-reaching hydrological process in the vadose zone. *J. of Contam. Hydrol.*, 1988, **3**, 207–226.
17. Grennholtz, D. E., Yeh, T.-C. J., Nash, M. S. B. and Wierenga, P. J. Geostatistical analysis of soil hydrological properties in a field plot. *J. of Contam. Hydrol.*, 1988, **3**, 227–250.
18. Greminger, P. J., Sud, Y. K. and Nielsen, D. R. Spatial variability of field-measured soil–water characteristics. *Soil Sci. Soc. Am. J.*, 1985, **49**, 1075–1082.
19. Gutjahr, A. L., Fast Fourier transforms for random field generation. Project Report for Los Alamos Grant to New Mexico Tech, Contract number 4-R58-2690R, Department of Mathematics, New Mexico Tech, Socorro, New Mexico, 1989.
20. Haan, C. T., *Statistical Methods in Hydrology*. Iowa State University Press, Ames, Iowa, 1977, 378 pp.
21. Harter, T. and Yeh, T. C. J. An efficient method for simulating steady unsaturated flow in random porous media: using an analytical perturbation solution as initial guess to a

- numerical model. *Water Resour. Res.*, 1993, **29**, 4139–4149.
22. Harter, T., Unconditional and conditional simulation of flow and transport in heterogeneous, variably saturated porous media. Ph.D. dissertation, University of Arizona, 1994.
  23. Harter, T. and Yeh, T.-C. J. Stochastic analysis of solute transport in heterogeneous, variably saturated porous media. *Water Resour. Res.*, 1996, **32**, 1585–1595.
  24. Harter, T. and Yeh, T.-C. J. Conditional stochastic analysis of solute transport in heterogeneous, variably saturated soils. *Water Resour. Res.*, 1996, **32**, 1597–1609.
  25. Hillel, D., *Fundamentals of Soil Physics*. Academic Press, New York, 1980, 413 pp.
  26. Hopmans, J. W., Schukking, H. and Torfs, P. J. J. F. Two-dimensional steady state unsaturated water flow in heterogeneous soils with autocorrelated soil hydraulic properties. *Water Resour. Res.*, 1988, **24**, 2005–2017.
  27. Kalos, M. H. and Whitlock, P.A., *Monte Carlo Methods*, vol. 1. Wiley, New York, 1986, 186 pp.
  28. Lauren, J. G., Wagenet, R. J., Bouma, J. and Wonston, J. H. M. Variability of saturated hydraulic conductivity in a glosaquitic hapludalf with macropores. *Soil Sci.*, 1988, **145**, 2005–2017.
  29. Mantoglou, A. and Gelhar, L. W. Stochastic modeling of large-scale transient unsaturated flow systems. *Water Resour. Res.*, 1987, **23**, 37–46.
  30. Mantoglou, A. and Gelhar, L. W. Capillary tension head variance, mean soil moisture content, and effective specific soil moisture capacity of transient unsaturated flow in stratified soils. *Water Resour. Res.*, 1987, **23**, 47–56.
  31. Mantoglou, A. and Gelhar, L. W. Effective hydraulic conductivities of transient unsaturated flow in stratified soils. *Water Resour. Res.*, 1987, **23**, 57–67.
  32. Mizell, S. A., Gutjahr, A. L. and Gelhar, L. W. Stochastic analysis of spatial variability in two-dimensional steady groundwater flow assuming stationary and nonstationary heads. *Water Resour. Res.*, 1982, **18**, 1053–1067.
  33. McCord, J. T., Stephens, D. B. and Wilson, J.L. Hysteresis and state-dependent anisotropy in modeling unsaturated hillslope hydrologic processes. *Water Resour. Res.*, 1991, **27**, 1501–1518.
  34. Moreno, L., Tsang, Y. W., Tsang, C. F., Hale, F. V. and Neretnieks, I. Flow and tracer transport in a single fracture: a stochastic model and its relation to some field observations. *Water Resour. Res.*, 1989, **24**, 2033–2048.
  35. Moreno, L. and Tsang, C. F. Flow channeling in strongly heterogeneous porous media: A numerical study. *Water Resour. Res.*, 1994, **30**, 1421–1430.
  36. Neuman, S. P., Stochastic approach to subsurface flow and transport: a view to the future. In: Proceedings, Workshop on Stochastic Subsurface Hydrology, Paris, January 1995.
  37. Nielsen, D. R., Biggar, J. W. and Erh, K. T. Spatial variability of field measured soil–water properties. *Hilgardia*, 1973, **42**, 215–260.
  38. Polmann, D. J., McLaughlin, D., Luis, S., Gelhar, L. W. and Ababou, R. Stochastic modeling of large-scale flow in heterogeneous unsaturated soils. *Water Resour. Res.*, 1991, **27**, 1447–1458.
  39. Press, W. H., Vetterling, W. T., Teukolsky, S.A. and Flannery, B.P., *Numerical Recipes in FORTRAN*, 2nd edn. Cambridge University Press, Cambridge, 1992.
  40. Priestley, M. B., *Spectral Analysis and Time Series*. Academic Press, San Diego, pp. 890, 1981.
  41. Roth, K. Steady state flow in an unsaturated, two-dimensional, macroscopically homogeneous Miller-similar medium. *Water Resour. Res.*, 1995, **31**, 2127–2140.
  42. Rubin, Y. Stochastic modeling of macrodispersion in heterogeneous porous media. *Water Resour. Res.*, 1990, **26**, 114–133.
  43. Russo, D. Stochastic analysis of simulated vadose zone solute transport in a vertical cross section of heterogeneous soils during nonsteady water flow. *Water Resour. Res.*, 1991, **27**, 267–284.
  44. Russo, D. Stochastic modeling of macrodispersion for solute transport in a heterogeneous unsaturated porous formation. *Water Resour. Res.*, 1993, **29**, 383–397.
  45. Russo, D. Stochastic modeling of solute flux in a heterogeneous partially saturated porous formation. *Water Resour. Res.*, 1993, **29**, 1731–1744.
  46. Ünlü, K., Nielsen, D. R. and Biggar, J. W. Stochastic analysis of unsaturated flow: one-dimensional Monte Carlo simulations and comparisons with spectral perturbation analysis and field observations. *Water Resour. Res.*, 1990, **26**, 2207–2218.
  47. Van Genuchten, M. Th. A closed-form equation for predicting the hydraulic conductivity of unsaturated soils. *Soil Sci. Soc. Am. J.*, 1980, **44**, 892–898.
  48. Vieira, S. R., Nielsen, D. R. and Biggar, J. W. Spatial variability of field measured infiltration rate. *Soil Sci. Soc. Am. J.*, 1981, **45**, 1040–1048.
  49. White, I. and Sully, M. J. On the variability and use of the hydraulic conductivity  $\alpha$  parameter in stochastic treatments of unsaturated flow. *Water Resour. Res.*, 1992, **28**, 209–213.
  50. Wierenga, P. J., Toorman, A. F., Hudson, D.B., Vinson, J., Nash, M. and Hills, R.G., Soil physical properties at the Las Cruces trench site, UREG/CR-5441, 1989.
  51. Wierenga, P. J., Hills, R. G. and Hudson, D. B. The Las Cruces trench site: characterization, experimental results, and one-dimensional flow. *Water Resour. Res.*, 1991, **27**, 2695–2706.
  52. Wilson, L. G. and De Cook, K. J. Field observations on changes in the subsurface water regime during influent seepage in the Santa Cruz River. *Water Resour. Res.*, 1968, **4**, 1219–1234.
  53. Yeh, T.-C. J., Gelhar, L. W. and Gutjahr, A. L. Stochastic analysis of unsaturated flow in heterogeneous soils, 1: statistically isotropic media. *Water Resour. Res.*, 1985, **21**, 447–456.
  54. Yeh, T.-C. J., Gelhar, L. W. and Gutjahr, A. L. Stochastic analysis of unsaturated flow in heterogeneous soils, 2: statistically anisotropic media with variable,  $\alpha$ . *Water Resour. Res.*, 1985, **21**, 457–464.
  55. Yeh, T.-C. J., Gelhar, L. W. and Gutjahr, A. L. Stochastic analysis of unsaturated flow in heterogeneous soils, 3: observations and applications. *Water Resour. Res.*, 1985, **21**, 465–471.
  56. Yeh, T.-C. J. One-dimensional steady state infiltration in heterogeneous soils. *Water Resour. Res.*, 1989, **25**, 2149–2158.
  57. Yeh, T.-C. J., Srivastava, R., Guzman, A. and Harter, T. A numerical model for two-dimensional water flow and chemical transport. *Ground Water*, 1993, **32**, 2–11.
  58. Yeh, T.-C. J. and Zhang, J. A geostatistical inverse method for variably saturated flow in the vadose zone. *Water Resour. Res.*, 1996, **32**, 2757–2766.
  59. Yevjevich, V. M., *Stochastic Processes in Hydrology*. Water Resources Publications, Fort Collins, CO, 1972.
  60. Zaslavsky, D. and Sinai, G. Surface hydrology, IV. Flow in sloping layered soil. *J. Hydraul. Div. Am. Soc. Civ. Engng.*, 1981, **107**(HY1), 53–64.

## APPENDIX A

A derivation of the spectral moments is given in Yeh et al.<sup>53,54</sup> assuming that  $\alpha$  is normally distributed. The analysis

here, however, assumes that  $\alpha$  is lognormally distributed. Writing  $\exp(A + a') = \exp(A) \exp(a')$ , expanding the exponential perturbation term in a Taylor series, truncating the Taylor series to first-order, and neglecting second- and higher-order terms, the first-order perturbation approximation of the unsaturated hydraulic conductivity is

$$Y + y' = (F + H\Gamma) + (f' + \Gamma h' + H\Gamma a'), \quad (\text{A1})$$

where  $\Gamma \equiv \exp(A)$ . Following the analysis of Yeh et al.<sup>53,54</sup> for gravity flow, the spectral solution for  $h'$ ,  $dZ_{h'}$ , then becomes

$$dZ_{h'} = \frac{ik_z(dZ_{f'} + H\Gamma dZ_{a'})}{(k_x^2 + k_z^2 - i\Gamma k_z)} \quad (\text{A2})$$

where  $dZ_{f'}$  and  $dZ_{a'}$  are the spectral representations of  $f'$  and  $a'^{40}$ . The spectral and cross-spectral density functions  $S_{pq}(k)$ , for pressure head, hydraulic conductivity and flux perturbations in the special case of identical correlation functions in  $f$  and  $a$  are:

$$S_{hh} = \frac{k_z^2}{(k_x^2 + k_z^2)^2 + \Gamma^2 k_z^2} [1 + 2\rho\zeta H\Gamma + (\zeta H\Gamma)^2] S_{ff} \quad (\text{A3})$$

$$S_{fh} = [-\Gamma k_z^2 + ik_z(k_x^2 + k_z^2)] \frac{(S_{ff} + H\Gamma S_{fa})}{(k_x^2 + k_z^2)^2 + (\Gamma^2 k_z^2)} \quad (\text{A4})$$

$$S_{ah} = \frac{\zeta\rho + \zeta^2 H\Gamma}{1 + \zeta\rho H\Gamma} S_{fh} \quad (\text{A5})$$

$$S_{yy} = \left[ 1 + \frac{-k_z^2 \Gamma^2}{(k_x^2 + k_z^2)^2 + \Gamma^2 k_z^2} \right] [1 + 2\rho\zeta H\Gamma + (\zeta H\Gamma)^2] S_{ff} \quad (\text{A6})$$

$$S_{qx.qx} = K_m^2 \frac{k_x^2 k_z^2}{(k_x^2 + k_z^2)^2 + \Gamma^2 k_z^2} [1 + 2\rho\zeta H\Gamma + (\zeta H\Gamma)^2] S_{ff} \quad (\text{A7})$$

$$S_{qz.qz} = K_m^2 \left[ 1 - \frac{k_z^2(\Gamma^2 + k_z^2) + 2k_x^2 k_z^2}{(k_x^2 + k_z^2)^2 + \Gamma^2 k_z^2} \right] \\ \times [1 + 2\rho\zeta H\Gamma + (\zeta H\Gamma)^2] S_{ff}.$$

$S_{ff}$  and  $S_{aa}$  may be obtained analytically or by numerical integration from the assumed covariance functions<sup>3,32</sup>.

The cross-spectral density  $S_{fa}$  depends on the desired cross-correlation between  $f(x)$  and  $a'(x + \xi)$ . If  $C_{aa}/\sigma_a^2 = C_{ff}/\sigma_f^2$ , i.e. the correlation functions of  $a'$  and  $f'$  are identical, then

$$S_{aa} = \zeta^2 S_{ff} \quad (\text{A8})$$

$$S_{af} = \zeta\rho S_{ff}.$$

In this study, all spectrally derived covariances and cross-covariances except those for  $f$  and  $a$ , are evaluated numerically through an inverse fast Fourier transform (inverse FFT<sup>5,39</sup>) of the spectral density functions in Appendix A. For the inverse FFT,  $S_{pq}(k)$  is discretized such that the two-dimensional covariance  $C_f(\xi)$  of  $f$  has 10 grid-points per  $\lambda_f$ . It is evaluated at all  $\xi \leq 100\lambda_f$ .